NOTAS DE FÍSICA

VOLUME IX

Nº 7

ON THE DIFFRACTION OF A PULSE BY A HALF-PLANE

by

R. C. T. da Costa

CENTRO BRASILEIRO DE PESQUISAS FÍSICAS

Av. Wenceslau Braz, 71

RIO DE JANEIRO

1962

Notas de Física - Volume IX - Nº 7

ON THE DIFFRACTION OF A PULSE BY A HALF-PLANE *

R. C. T. da Costa
Centro Brasileiro de Pesquisas Físicas
and Faculdade Nacional de Filosofia, Rio de Janeiro

(Received March 12, 1962)

Summary. The physical properties of the solution in the diffraction of an electromagnetic pulse by a perfectly conducting half-plane are studied from the standpoint of energy propagation. The form of the energy current lines and of the level lines of the energy density is given, for several instants of time after the arrival of the main part of the incident pulse at the half-plane. The splitting of the incident wave front into a transmitted and a reflected one leads to the formation of an energy reservoir near the edge. The energy contained in this reservoir is then reemitted, giving rise to the diffracted pulse. Lines of zero energy current play an important role in this process; their formation and evolution is discussed, as well as the growth of the diffracted wave front. The asymptotic behaviour of the diffracted pulse for large times is considered.

---

* To appear in Il Nuovo Cimento.

1. Introduction.

The role of energy accumulation effects in diffraction theory has been discussed in a previous paper[1], in connection with the diffraction of a pulse at the open end of a parallel-plate wave guide. However, a detailed study of the accumulation process was not possible in this case, owing to the mathematical complexity of the solution.

The simplest problem in diffraction theory in which these effects can be investigated is the well-known problem of the diffraction of a pulse by a perfectly conducting half-plane. The solution of this problem was given by Sommerfeld[2] and Lamb[3] (cf. also Friedlander[4]). It also enables us to discuss the initial stages of the diffraction process in the above-mentioned waveguide problem, because the two plates behave in a completely independent way before the diffracted wave originating from one of them reaches the other one[5].

Although the mathematical solution of the half-plane problem has been known for a long time, its physical properties do not seem to have been fully investigated. These properties can best be studied by considering the propagation of energy, as was done by Braunbek and Laukien[6] in the monochromatic case. This case, however, is not well suited for our purpose, because the energy accumulation effects are not clearly apparent in the stationary solution.

In the present paper, we shall study the energy flow

as a function of time, in the diffraction of a pulse by a half-plane. The solutions are given in section 2, both for a Cauchy-type incident pulse of width b and for a delta-type incident pulse, which can be considered as a limiting case of the former one as $b \longrightarrow 0$.

In section 3, the energy current lines and the level lines of the energy density, for a delta-type incident pulse, are studied. Although the behaviour at the wave fronts is strongly singular, the solution can be physically interpreted as representing the asymptotic behaviour, for large times, of the solution for a pulse of finite width, and it has the advantage of being considerably simpler. A striking feature of the solutions is the appearance of lines where the energy current vanishes. These lines separate regions where the energy flows in opposite directions.

The effects due to the finite width of the incident pulse are discussed in section 4, in the case of a Cauchy-type pulse of width b. The energy flow pattern is drawn for $t = b/c$ and for $t = 10\ b/c$. The formation and development of the zero-energy-current lines, the growth of the diffracted wave front, and the energy accumulation near the edge, are discussed.

The junctions between the geometrical and diffracted wave fronts and the zero-energy-current lines give rise to very rapid variations in the energy flow. These regions are studied in section 5.

Finally, in section 6, the behaviour of the energy reservoir near the edge, as a function of time, is discussed in

detail.

The conclusions will be found in section 7.

2. Formulation of the problem.

The coordinate system is shown in fig. 1. The perfectly conducting half-plane is represented by $x > 0$, $y = 0$, and the incident pulse travels in the direction of the negative y-axis. We shall consider only the case of transverse magnetic waves, which can be described by a scalar function $u(x, y, t)$. The field components are

$$\vec{H} = (0, 0, u), \quad \vec{E} = (E_x, E_y, 0), \tag{1}$$

with the boundary condition $E_x = 0$ for $x > 0$, $y = 0$.

The problem has also an acoustical analogue, if we interpret $u(x, y, t)$ as the velocity potential of sound waves; the boundary condition then describes a perfectly rigid half-plane. However, only the electromagnetic interpretation will be considered in this work.

The solution for an incident pulse of arbitrary shape, and for both polarizations, was given by Lamb[3], who considered in detail the case in which the incident pulse is of the form of a Cauchy wave packet,

$$u_i = \frac{b}{b^2+(ct+y)^2} . \tag{2}$$

This represents a pulse of half-width $2b$ centered at $y = -ct$.

The corresponding solution for transverse magnetic polarization is

$$H_z = u = \frac{1}{2}\mathcal{R}\left\{ \frac{1}{b+i(ct+y)} + \frac{1}{b+i(ct-y)} + \frac{e^{-i\pi/4}}{[b+i(ct-r)]^{\frac{1}{2}}} \times \right.$$

$$\left. \times \left[\frac{\xi+\eta}{b+i(ct+y)} + \frac{\xi-\eta}{b+i(ct-y)} \right] \right\}, \qquad (3)$$

where $\xi = r^{\frac{1}{2}} \cos \theta/2$, $\eta = r^{\frac{1}{2}} \sin \theta/2$, and $[b+i(ct-r)]^{\frac{1}{2}}$ is taken to be positive for $ct = r$. The polar coordinate system is shown in fig. 1.

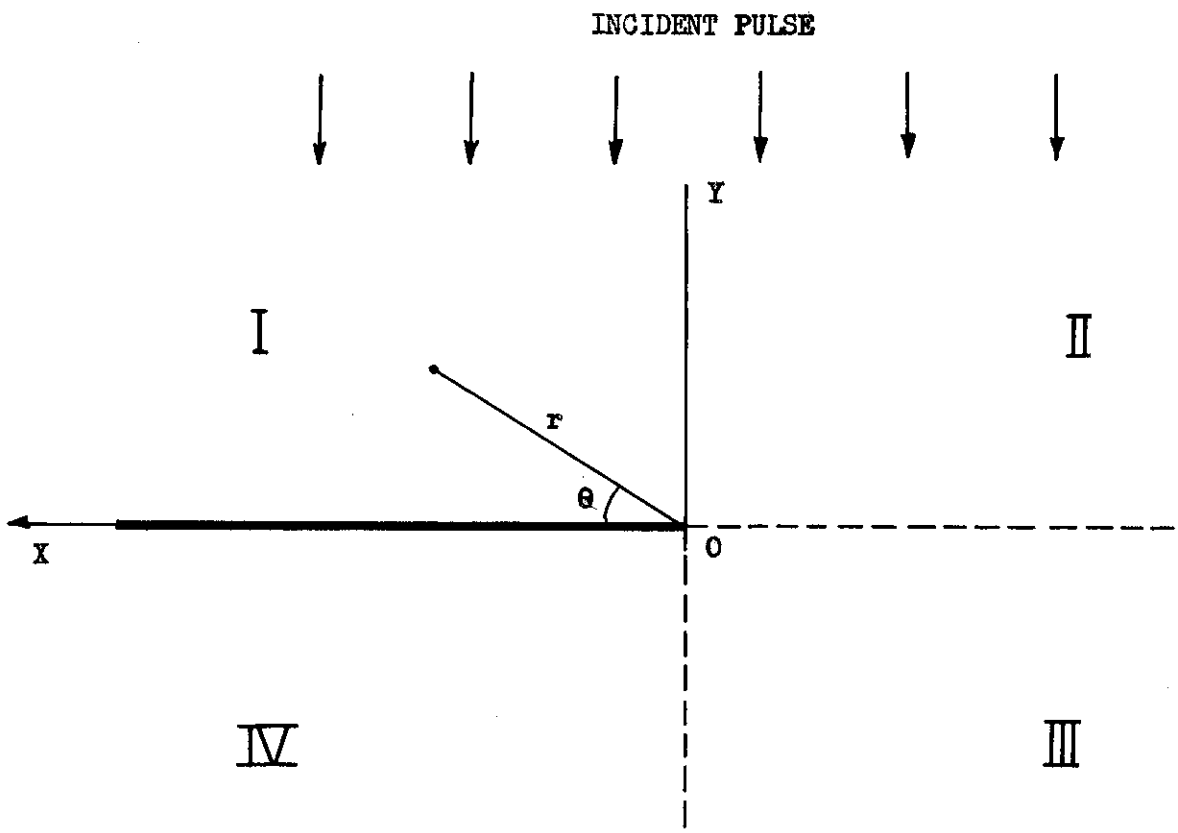

Fig. 1 - The coordinate system.

The electric field components can easily be derived from (3). The results are:

$$E_r = \tfrac{1}{2}\Re\left\{\cos\theta\left[\frac{1}{b+i(ct+y)} - \frac{1}{b+i(ct-y)}\right] + \right.$$

$$\left. + \frac{e^{i\pi/4}}{r}\cdot\left[b+i(ct-r)\right]^{\frac{1}{2}}\cdot\left[\frac{\xi-\eta}{b+i(ct+y)} - \frac{\xi+\eta}{b+i(ct-y)}\right]\right\}, \qquad (4)$$

$$E_\theta = \tfrac{1}{2}\Re\left\{\sin\theta\left[\frac{1}{b+i(ct-y)} - \frac{1}{b+i(ct+y)}\right] - \right.$$

$$\left. - \frac{e^{i\pi/4}}{r}\,\frac{b+ict}{\left[b+i(ct-r)\right]^{\frac{1}{2}}}\left[\frac{\xi+\eta}{b+i(ct+y)} + \frac{\xi-\eta}{b+i(ct-y)}\right]\right\}. \qquad (5)$$

We shall also consider a delta-type incident pulse,

$$u_i = \delta(ct+y) = \lim_{b\to 0}\left[\frac{1}{\pi}\,\frac{b}{b^2+(ct+y)^2}\right]. \qquad (6)$$

It might appear, at first sight, that such a pulse is of a too singular character for a physical interpretation of the corresponding solution to be possible. It is certainly true that quadratic functions of the field components, such as the energy density and the energy current, become highly singular at the wave fronts associated with (6). However, it will be shown later that the corresponding solution, behind the diffracted wave front, is closely related with the asymptotic behaviour of the diffracted

wave originated from the pulse (2), for times $t \gg b/c$, so that the results have a direct physical interpretation. The main reason for considering a delta-type incident pulse is the particularly simple character of the solution in this case.

According to (6), the solution can be derived from (3), (4) and (5), by going over to the limit $b \longrightarrow 0$ and taking into account the normalization factor $1/\pi$. The solution can be written as the sum of a geometrical optics term and a diffracted term. For $t < 0$, the solution is obviously given just by the incident wave:

$$H_z = E_x = \delta(ct+y) \qquad (t<0). \tag{7}$$

The incident pulse reaches the half-plane at $t = 0$.

For $t > 0$, the solution can be written as

$$u = u_t + u_r + u_d, \tag{8}$$

where u_t and u_r, the transmitted pulse and the reflected pulse, are the geometrical optics terms, and u_d is the diffracted wave.

The transmitted pulse is given by

$$H_{z,t} = E_{x,t} = \begin{cases} \delta(ct+y) & \text{in region III,} \\ 0 & \text{in region IV,} \end{cases} \tag{9}$$

and the reflected pulse is given by

$$H_{z,r} = -E_{x,r} = \begin{cases} \delta(y-ct) & \text{in region I,} \\ 0 & \text{in region II.} \end{cases} \tag{10}$$

The division into regions is shown in fig. 1.

It is clear, from considerations of causality, that the diffracted wave vanishes for $r > ct$. For $r < ct$ it is given by

$$H_{z,d} = -\frac{1}{2\pi(ct-r)^{\frac{1}{2}}}\left(\frac{\xi+\eta}{ct+y}+\frac{\xi-\eta}{ct-y}\right), \tag{11}$$

$$E_{r,d} = -\frac{(ct-r)^{\frac{1}{2}}}{2\pi r}\left(\frac{\xi+\eta}{ct-y}-\frac{\xi-\eta}{ct+y}\right), \tag{12}$$

$$E_{\theta,d} = -\frac{ct}{2\pi r(ct-r)^{\frac{1}{2}}}\left(\frac{\xi+\eta}{ct+y}+\frac{\xi-\eta}{ct-y}\right). \tag{13}$$

The field becomes singular both for $r \longrightarrow ct$ and for $r \longrightarrow 0$. The former singularity is the characteristic $(ct-r)^{-\frac{1}{2}}$ singularity associated with the free propagation of a cylindrical pulse, which may also be regarded as the effect of an instantaneous excitation in a point of a two-dimensional space[7]. The "tail" of the diffracted pulse is a well-known feature of two-dimensional wave propagation. In the present case, the incident pulse gives rise to an instantaneous excitation at $t = 0$, along the edge of the half-plane. The corresponding energy accumulation behind the diffracted wave front should therefore be regarded as arising from the two-dimensional nature of the problem.

The $r^{-\frac{1}{2}}$ singularity of the electric field for $r \longrightarrow 0$ is a general feature of the solution, which is independent of the shape of the incident pulse (cf. (4), (5), (12) and (13)). This is the characteristic singularity at a sharp edge, which is also found in the monochromatic solution[8]. The nature of the energy

accumulation in the neighbourhood of the edge is entirely different from that which takes place behind the wave front, and it will be one of the main objects of our study in the following sections.

3. Delta-type incident pulse.

We shall consider, in the first place, the case of a delta-type incident pulse. According to (11), (12) and (13), all components of the diffracted field are of the form

$$(ct)^{-1} f(r/ct, \theta).$$

Thus, the lines of force in the diffracted wave expand radially (in the two-dimensional sense) with velocity c. The Poynting vector $\vec{S}$ and the energy density W are of the form

$$\vec{S} = \frac{c}{4\pi} \vec{E} \times \vec{H} = \frac{c}{16\pi} (ct)^{-2} \vec{\mathcal{S}}(r/ct, \theta), \qquad (14)$$

$$W = \frac{1}{8\pi} \left(\vec{E}^2 + \vec{H}^2 \right) = \frac{1}{32\pi} (ct)^{-2} \mathcal{W}(r/ct, \theta). \qquad (15)$$

The energy contained in a volume element which is undergoing radial expansion with velocity c,

$$r\, dr\, d\theta\, dz = (ct)^2 (r/ct)\, d(r/ct)\, d\theta\, dz,$$

remains constant in time, provided we acompany the volume element during its expansion.

The form of the energy current lines (solid lines with arrowheads) and the level lines of energy density (dashed lines), for an arbitrary instant of time $t > 0$, is shown in fig. 2. To draw these lines, the energy density and the slope of the Poynting vector were evaluated at points $(r/ct, \theta)$, for $r/ct = 0.1, 0.2, 0.5, 0.8$ and 0.9, and for θ varying from $0°$ to $360°$ in steps of $15°$. The number assigned to each dashed line is the corresponding value of $\mathcal{W}(r/ct, \theta)$ in arbitrary units. According to what we have seen above, the form of the lines at any other instant of time can be obtained by radially expanding or contracting fig. 2 by an appropriate factor.

Notice that, insofar as the diffracted wave is concerned, the pattern is completely symmetrical with respect to the half-plane. The direction of incidence is indicated only by the position of the reflected and transmitted wave fronts.

Let us now consider the energy distribution. The energy accumulations near the diffracted wave front and in the neighbourhood of the edge of the half-plane, already referred to in the previous section, are immediately apparent in fig. 2. Another apparent feature of the energy distribution is its asymmetry with respect to the plane $x = 0$: the energy is much more concentrated in regions I and IV than in II and III. In the neighbourhood of the diffracted wave front, for instance, the energy density behaves like $(\cos \theta/2 \,/\, \cos \theta)^2$ (the divergence at $\theta = \pi/2$ or $3\pi/2$ is due to the junction with the geometrical wave fronts, which will be discussed later). This is identical to the angular distribution of Sommerfeld's so-

lution[9] for a monochromatic plane wave (transverse magnetic case). In the transverse electric case, the behaviour is just the opposite: the energy density in regions I and IV is much smaller than in II and III. This is due to the different boundary condition for this case, $\vec{E} = (0, 0, E_z) = 0$ for $x > 0$, $y = 0$, which implies the vanishing of the Poynting vector on the half-plane, and does not allow it to act as a waveguide.

Let us consider next the energy current lines. The most striking feature, in this respect, is the existence of lines (dotted lines in fig. 2) where the energy current vanishes. They are given by $H_z = 0$, and they separate regions where the energy flows in opposite directions. The origin and physical significance of these lines will be discussed in the next section.

Another feature which deserves attention is the behaviour of the solution near the diffracted wave front ($r \approx ct$), at the points $\theta = \pi/2$, $3\pi/2$, and π. These three points belong at the same time to the wave front (where $H_z \longrightarrow \infty$) and to the zero-Poynting-vector lines ($H_z = 0$). The first two of them also belong to the junction between the geometrical (plane) and the diffracted (cylindrical) wave fronts. Similar junctions appear in the theory of the Čerenkov effect, when a fast particle penetrates into a medium: in this case, the Čerenkov cone has to be joined to a spherical wave front. Clearly, these junctions can only be studied in the case of an incident pulse of finite width. This will be done in detail in section 5.

The velocity $\vec{v}$ of propagation of the energy may be de-

fined by

$$\vec{S} = \vec{v} W \ . \qquad (16)$$

The absolute value of the Poynting vector (which has not been represented in fig. 2) is then obtained by multiplying the energy density by the velocity. The velocity tends to zero on the lines $H_z = 0$, which were already mentioned above. In particular, it tends to zero at the edge of the half-plane. In the neighbourhood of the edge, the velocity is much smaller than c; the field has an electrostatic character, so that the energy accumulation in this zone is almost purely electrical in nature. Away from the lines $H_z = 0$, the velocity of propagation of the energy approaches c, so that the behaviour of the absolute value of the Poynting vector is quite similar to that of the energy density.

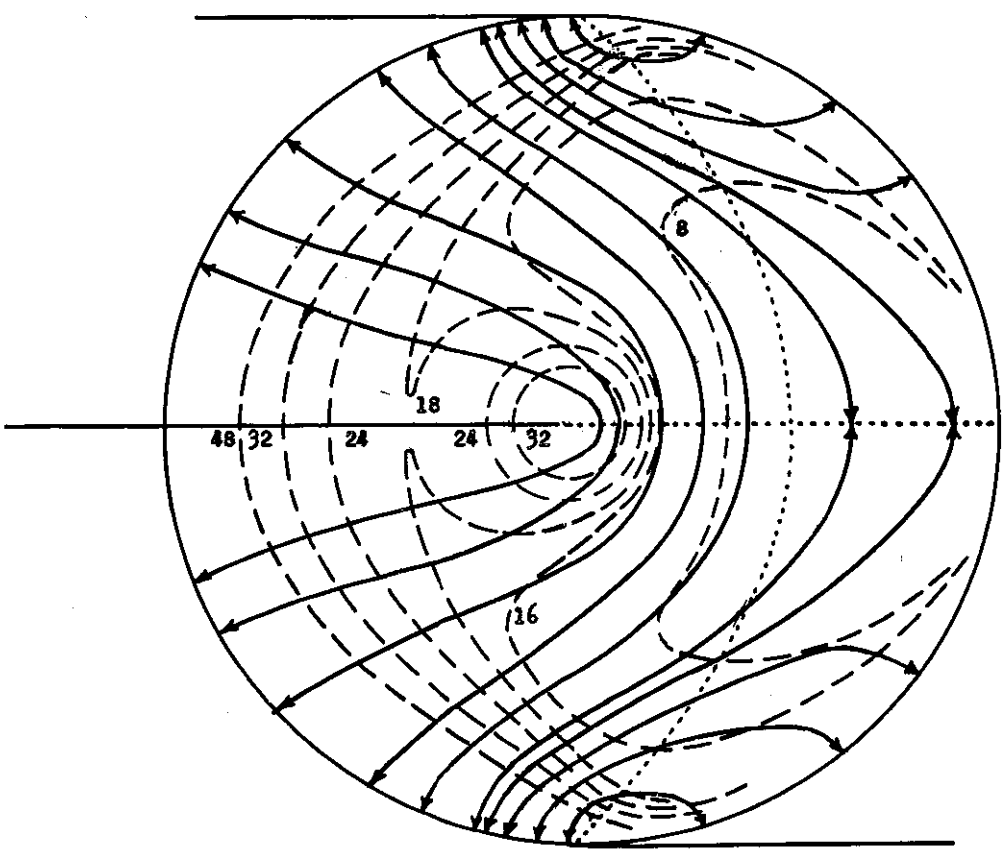

Fig. 2 - Energy flow pattern for a delta -type pulse:

——→ energy current lines.

—24— level line of energy density = 24 (in arbitrary units).

..... lines of zero energy current.

It must be kept in mind that, in this hydrodynamical description of the energy flow, the energy current lines correspond to stream lines in an unsteady flow; they should not be confused with trajectories.

4. Cauchy-type incident pulse.

We shall now consider the case of the incident pulse (2), the solution being given by (3), (4) and (5). It has already been mentioned in section 2 that the asymptotic behaviour of this solution for large times is closely related with the solution for a delta-type incident pulse. To show this, it suffices to notice that, for $ct - r \gg b$, we can neglect b in (3) to (5); according to (6), this is the same as going over to the solution for a delta-type pulse (except for the normalization factor $1/\pi$). Thus, the results of the previous section can also be interpreted as describing the behaviour of the diffracted wave for $ct \gg b$, at distances from the wave front also $\gg b$. The effects which we are now going to study are all due to the finite width of the pulse. For $ct \gg b$, these effects are all concentrated in the neighbourhood of the wave fronts, and they will be studied in section 5. It suffices, therefore, to consider values of ct of the order of b. Negative values of ct will not be considered, as they are related only to the diffraction of the head of the pulse, and do not lead to any interesting effects.

The energy current lines and the level lines of the

energy density for ct = b are shown in fig. 3. The conventions are the same as in fig. 2; we have also indicated the width of the transmitted and reflected pulses by means of the dashed lines $y = \pm ct \pm b$.

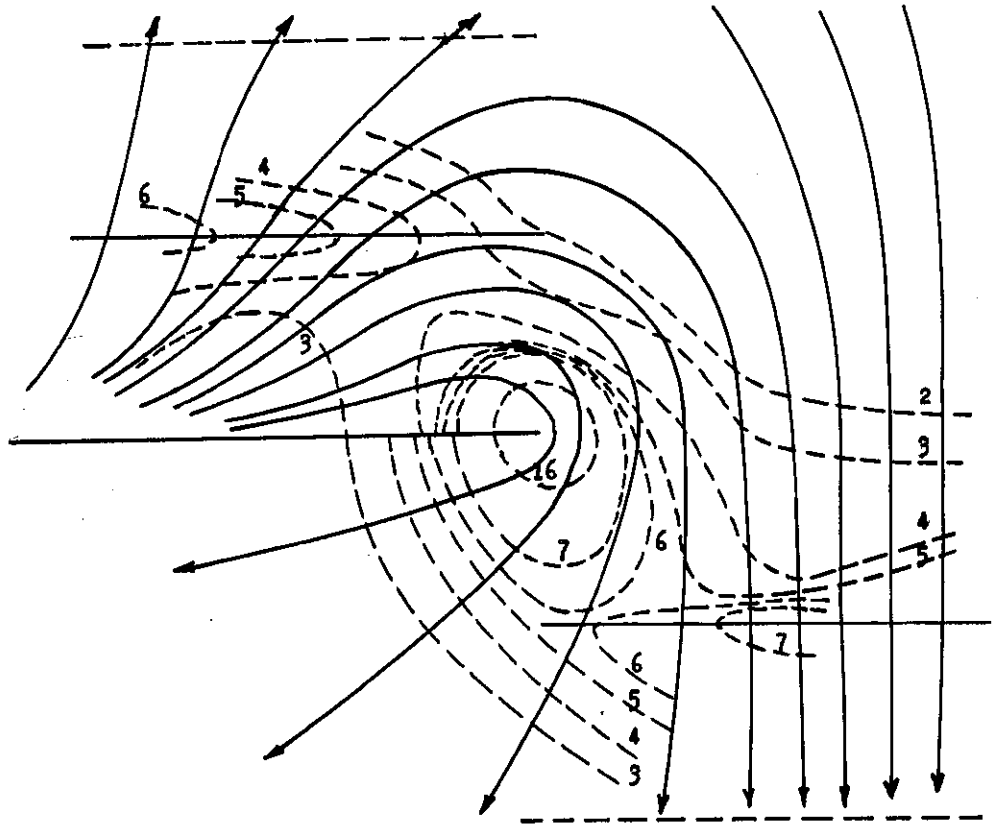

Fig. 3 - Energy flow pattern for a Cauchy-type pulse, ct = b;
——————→ energy current lines.
------^{2}------ level line of energy density = 2 (in arbitrary units).
—————— geometrical wave fronts.
— — — — — — lines y = ct + b and y = - ct - b.

The main difference between figures 2 and 3 is the absence, in the latter, of zero-Poynting-vector lines: there is no reversal of sense of the energy flow. The energy flows from regions I and II into regions III and IV ($H_z > 0$ everywhere). This smooth flow around the half-plane takes place during all negative times, while the energy accumulated near the edge builds up steadily, accompanying the increase in

value of the incident pulse. The reversal of the Poynting vector is related to the beginning of the backward radiation (depletion of the energy reservoir). We see that this reversal still has not taken place for $t = b/c$, although the incident pulse has already gone through its maximum.

In so far as the energy distribution is concerned, we can notice in fig. 3 that the energy accumulation near the edge occupies the whole region $r \lesssim ct$, which connects the geometrical (transmitted and reflected) wave fronts $y = \pm ct$. The diffracted wave front has not yet been formed. The energy density is also slightly greater in regions III and IV than in regions I and II.

The pattern for $ct = 10b$ is shown in fig. 4, where the same conventions as in figures 2 and 3 have been adopted. The numbers assigned to the level lines of the energy density are the corresponding values of $\mathcal{W}(r/ct, \theta)$ in the same units as in fig. 3, so that, according to (15), the energy associated with these lines is 100 times smaller than that associated with the corresponding lines of fig. 3.

In fig. 4 there already appear the two zero-Poynting-vector lines (dotted lines), which will tend to the asymptotic form shown in fig. 2 as ct increases (Cf. also fig. 5). These lines must therefore appear for $b/c < t < 10b/c$. It can be shown that they appear at two different instants of time. Each of them appears as an isolated point and thereafter it expands, remaining always closed, except where it comes in touch with the half-plane (this happens only for the line in region I).

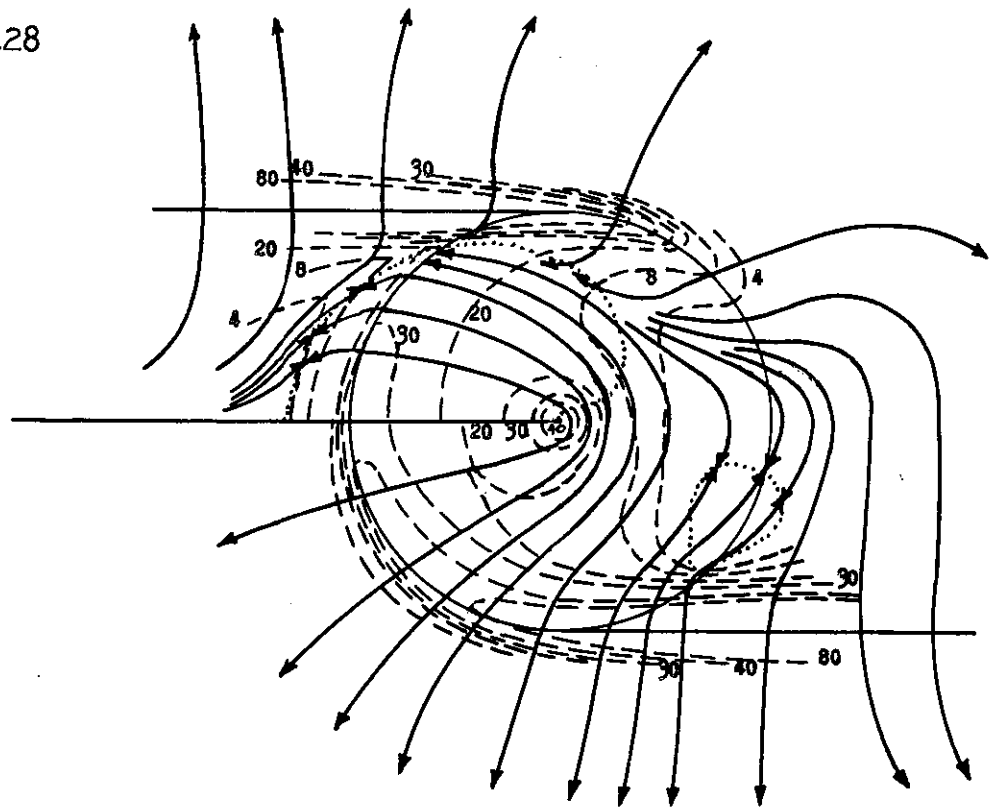

Fig. 4 - Energy flow pattern for a Cauchy-type pulse, ct = 10b:
——→ energy current lines.
----20---- level line of energy density = 20 (in arbitrary units.)
..... lines of zero energy current.
——— geometrical and diffracted wave fronts.

Although the Poynting vector vanishes along the closed lines, the energy contained within them is not constant, and increases with time. In fact, let us consider a cylindrical volume V_t, having one of the zero-Poynting-vector lines as its basis and with generators parallel to the z-axis. This volume will obviously increase with time. We have

$$\frac{d}{dt}\int_{V_t} W\,dV = \int_{S_t} W\,\vec{u}\cdot\vec{n}\,dS + \int_{V_t}\frac{\partial W}{\partial t}\,dV, \qquad (17)$$

where S_t is the surface of the cylinder, $\vec{n}$ its exterior normal and $\vec{u}$ the velocity of expansion of the surface. It follows

from

$$\operatorname{div} \vec{S} + \frac{\partial W}{\partial t} = 0 \ ,$$

and from the vanishing of $\vec{S}$ on the surface S_t, that the last integral of (17) vanishes. The remaining integral is always positive, which justifies the above statement.

The first zero-Poynting-vector line, which marks the beginning of the backward radiation, appears for $ct \approx 1.73b$, at the point $r \approx 0{,}66\ ct$, $\theta \approx 0°$. The other line appears for $ct \approx 7b$, at the point $r \approx 0{,}9\ ct$, $\theta \approx 210°$. There does not seem to be such a direct physical interpretation for this line as for the former one. It plays a far less important role, because it appears in a region where the energy density is very weak.

It can be verified that, immediately after their formation, both zero-Poynting-vector lines expand with a velocity greater than c. However, this does not lead to any difficulties, because, as shown above, the energy contained within the lines is not constant. The velocity of propagation of the energy can never exceed c. In fact, it follows from its definition (16) that[10]

$$16\pi^2 W^2 \left(1 - \frac{v^2}{c^2}\right) = \frac{1}{4}\left(\vec{E}^2 - \vec{H}^2\right) + \left(\vec{E}\cdot\vec{H}\right)^2 , \qquad (18)$$

so that $v \leq c$, and $v = c$ is only possible for $\vec{E}^2 = \vec{H}^2$, $\vec{E}\cdot\vec{H} = 0$ (wave zone).

The growth of the diffracted wave front, which still had not been formed in fig. 3, can already be noticed in fig. 4.

This growth is more pronounced in regions I and II than in III and IV.

In order to show the way in which the zero-Poynting-vector lines approach their asymptotic form of fig.2, these lines have been drawn in fig. 5 for ct = 100b. The only feature which differs appreciably from fig. 2 is the existence of a gap between the two lines, through which a communication is established between the energy current lines in regions II and III.

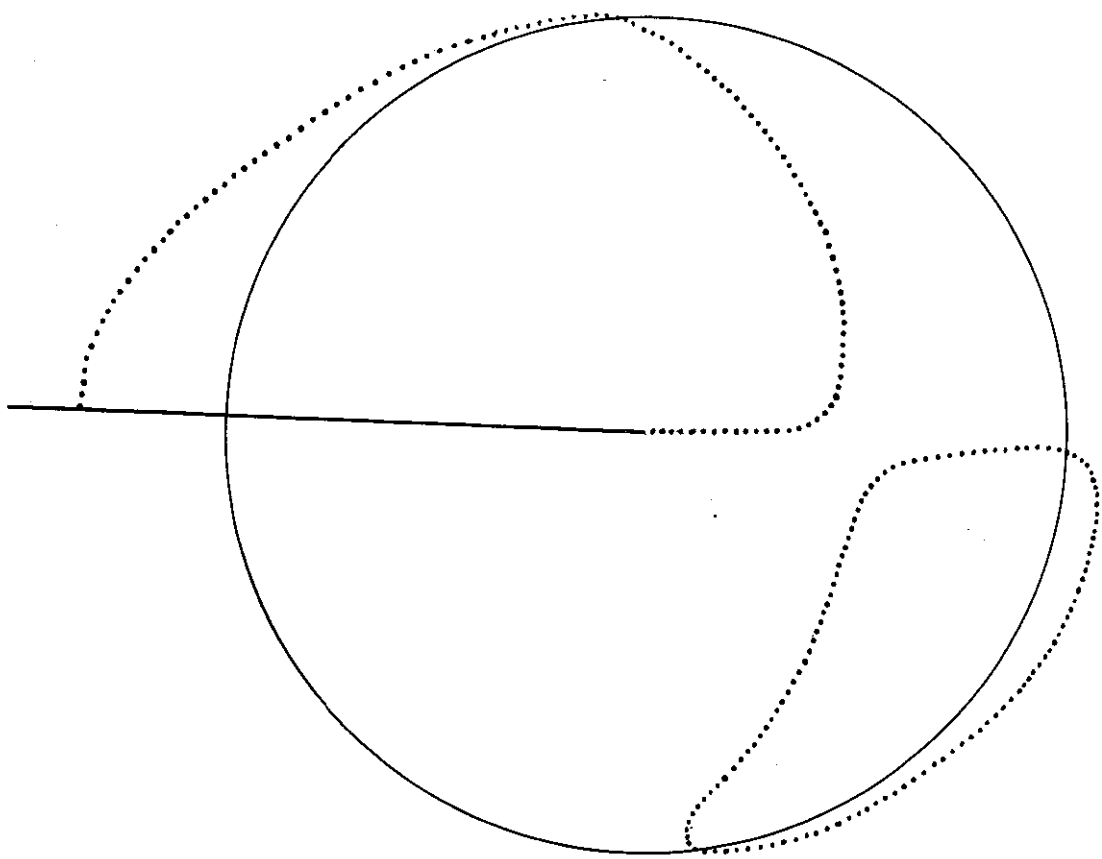

Fig. 5 - Lines of zero energy current for a Cauchy-type pulse, ct = 100b:
——————— diffracted wave front.
..... lines of zero energy current.

5. Junction Points.

There remains to consider the behaviour of the solution near the junction points at $r = ct$, $\theta = \pi/2$, $\theta = 3\pi/2$ and $\theta = \pi$. In the limiting case of a delta-type pulse, as we have seen in section 3, these points belong at the same time to at least one of the wave fronts ($H_z \longrightarrow \infty$), and to one of the zero-Poynting-vector lines ($H_z = 0$). Thus, for $ct \gg b$, we would expect to find very rapid variations in the energy flow near these points.

The junctions between the diffracted and geometrical wave fronts take place in circular segments, which are the intersections of the strips $ct - b \leqslant y \leqslant ct + b$ and $-ct - b \leqslant y \leqslant -ct + b$ with the circular ring $ct - b \leqslant r \leqslant ct + b$. These segments are the analogues, for the pulse (2), of the Fresnel diffraction region for the monochromatic solution.

The junctions with the reflected and transmitted wave fronts, for $ct = 100b$, are shown in figures 6 and 7, respectively. The zero-Poynting-vector lines are already very close to their limiting positions. Both the direction of the Poynting vector and the energy density change very rapidly across these lines. This behaviour can easily be understood. According to (3) and (5), $H_z \approx E_\theta$ for $ct \gg b$, $r \approx ct$ and $\theta \approx \pi/2$ or $3\pi/2$. Thus, near the zero-Poynting-vector lines ($H_z = 0$), we shall also have $E_\theta \approx 0$. On the other hand, the field near the diffracted wave front is nearly transverse, so that $E_r \ll E_\theta$. The sudden variation in the direction of the Poynting vector, on crossing the zero-Poynting-

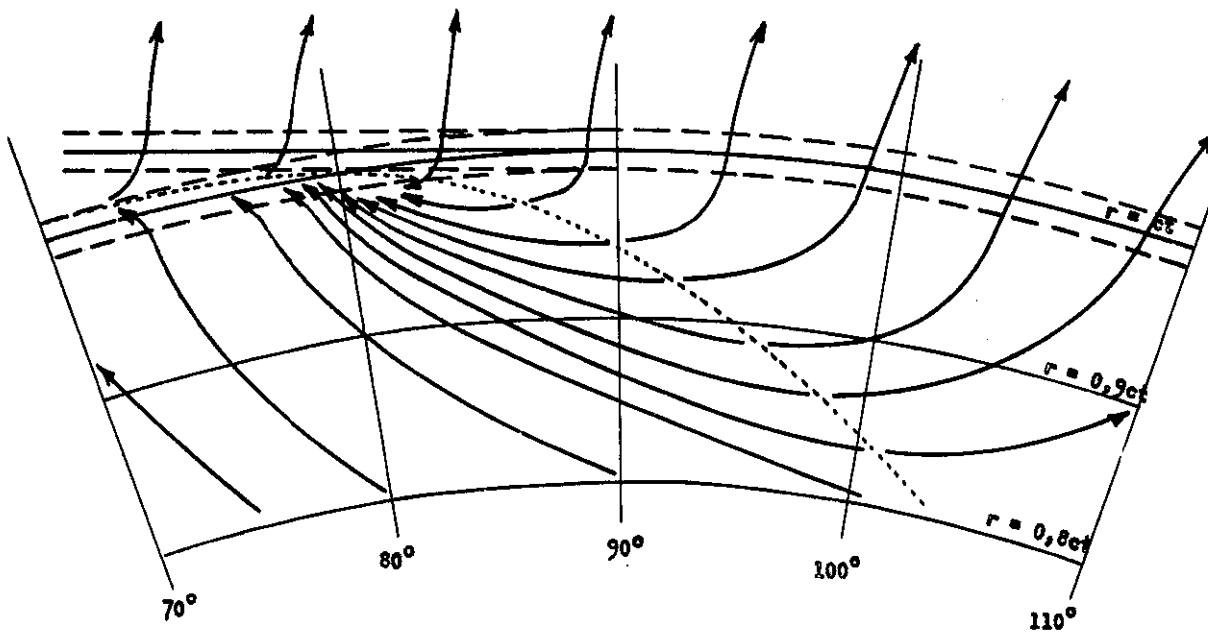

Fig. 6 - The junction between the diffracted and reflected wave fronts for a Cauchy-type pulse, ct = 100b:

——————→ energy current lines.
..... line of zero energy current.
– – – – – – – – – – – – – – – – lines r = ct ± b and y = ct ± b.

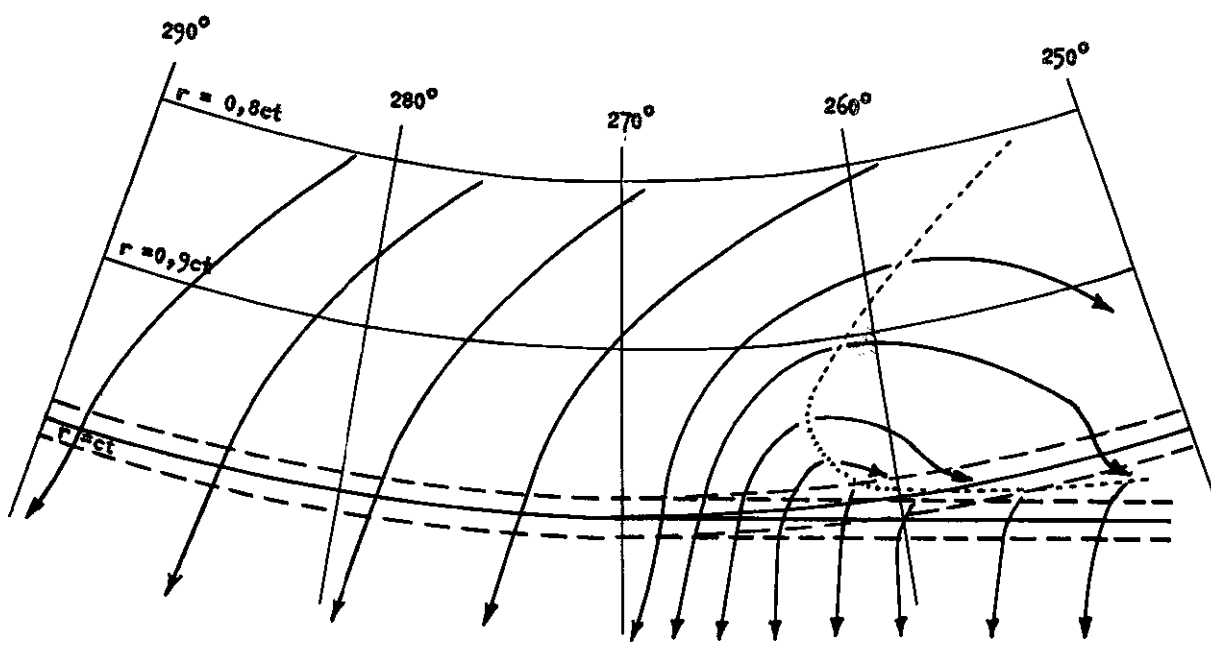

Fig. 7 - The junction between the diffracted and transmitted wave fronts for a Cauchy-type pulse, ct = 100b:

——————→ energy current lines.
..... line of zero energy current.
– – – – – – – – – – – – – – – – lines r = ct ± b and y = -ct ± b.

vector lines, is due to the sharp decrease of the E_θ component. The rapid change in the energy density is due to the same effect.

The behaviour of the energy density as a function of θ, in the neighbourhood of $\theta = \pi/2$, is shown in fig. 8. Both in this figure and in the former ones, the function $\mathcal{W}(r/ct, \theta)$ is represented instead of the energy density (Cf. (15)); the units employed are always the same. A logarithmic scale is employed in fig. 8, on account of the rapid variation of the energy density. The various minima, for different values of r/ct, appear in the vicinity of zero-Poynting-vector lines, as can be verified by comparison with fig. 6. The behaviour of the energy density in the neighbourhood of $\theta = 3\pi/2$ is very similar to that shown in fig. 8.

The behaviour of the solution near the point $r = ct$, $\theta = \pi$, where a zero Poynting vector line approaches the diffracted wave front, is shown in figures 9 and 10. According to fig. 10, there is a sharp minimum in the energy density for $\theta \approx \pi$. This corresponds to a gap in the diffracted wave front, which is still present for ct = 100b, showing that this is the last region of the wave front to be formed.

6. Energy accumulation near the edge.

We shall now consider the behaviour of the energy density as a function of time near the edge of the half-plane. It

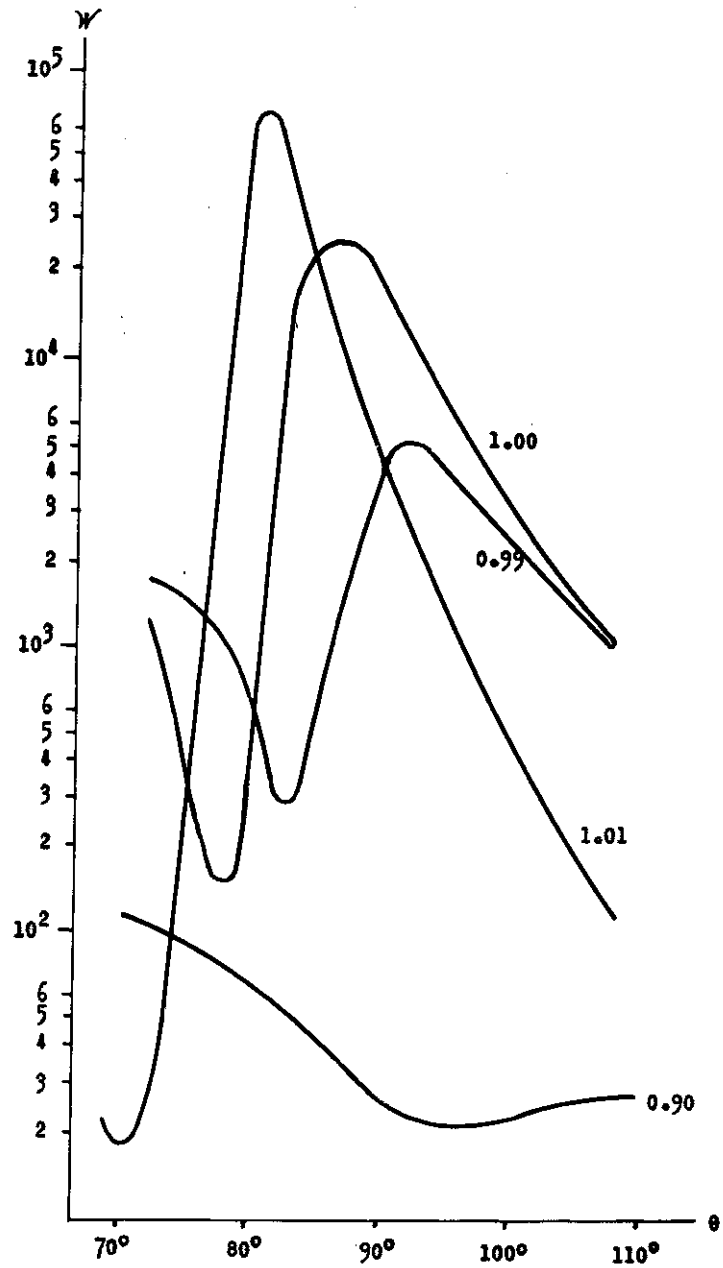

Fig. 8 - The energy density as a function of θ near θ = $\pi/2$, for different values of r/ct (indicated by the numbers beside the curves).

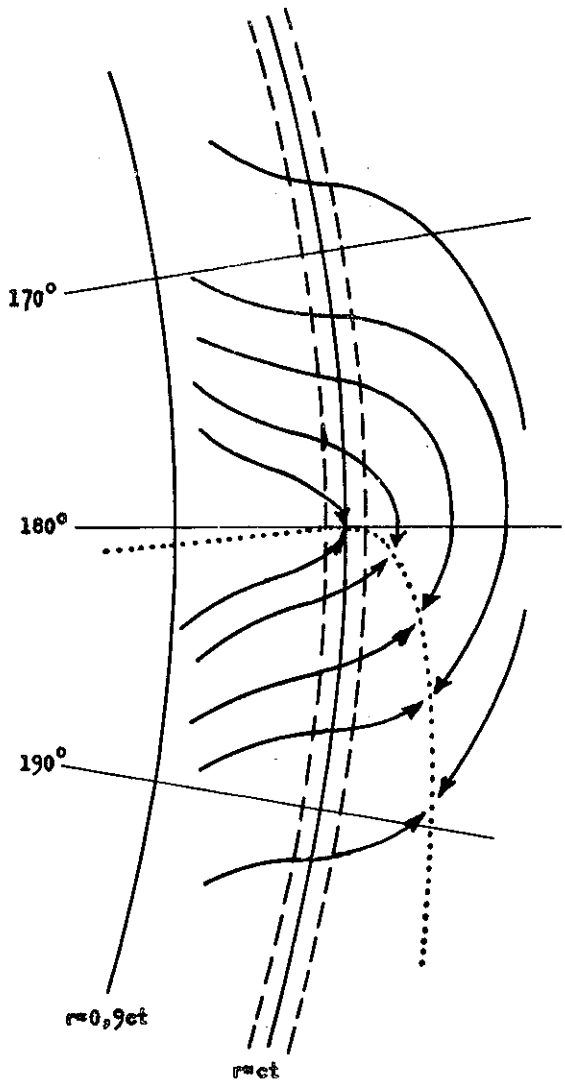

Fig. 9 - Energy flow pattern for a Cauchy-type pulse near $\theta = \pi$, $ct = 100b$:

——→ energy current lines.

..... line of zero energy current.

– – – – – – lines $r = ct \pm b$.

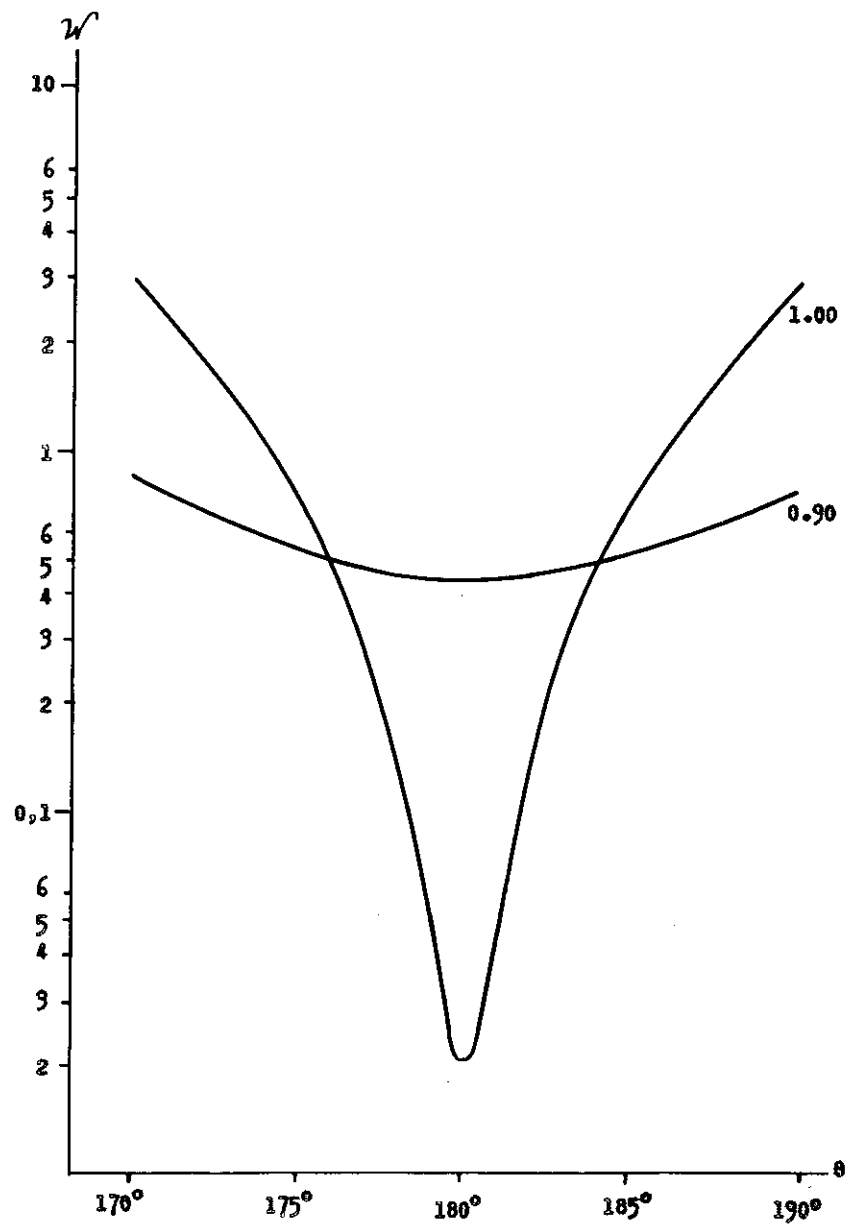

Fig. 10 - The energy density as a function of θ, near $\theta=\pi$, for different values of r/ct (indicated by the numbers beside the curves).

follows from (3), (4), (5) and (16) that, for $r \ll b$,

$$W = \frac{1}{16\pi r} \left(b^2 + c^2 t^2\right)^{-\frac{1}{2}} \left[1 + \frac{ct}{(b^2 + c^2t^2)^{\frac{1}{2}}}\right], \qquad (19)$$

$$\frac{v}{c} = 2^{3/2} \, b \sqrt{r} \left(b^2 + c^2t^2\right)^{-3/4} \left[1 + \frac{ct}{(b^2 + c^2t^2)^{\frac{1}{2}}}\right]^{-\frac{1}{2}}, \qquad (20)$$

where v, as before, is the velocity of propagation of the energy. The behaviour of (19) and (20) as a function of time is shown in figs. 11 and 12, respectively.

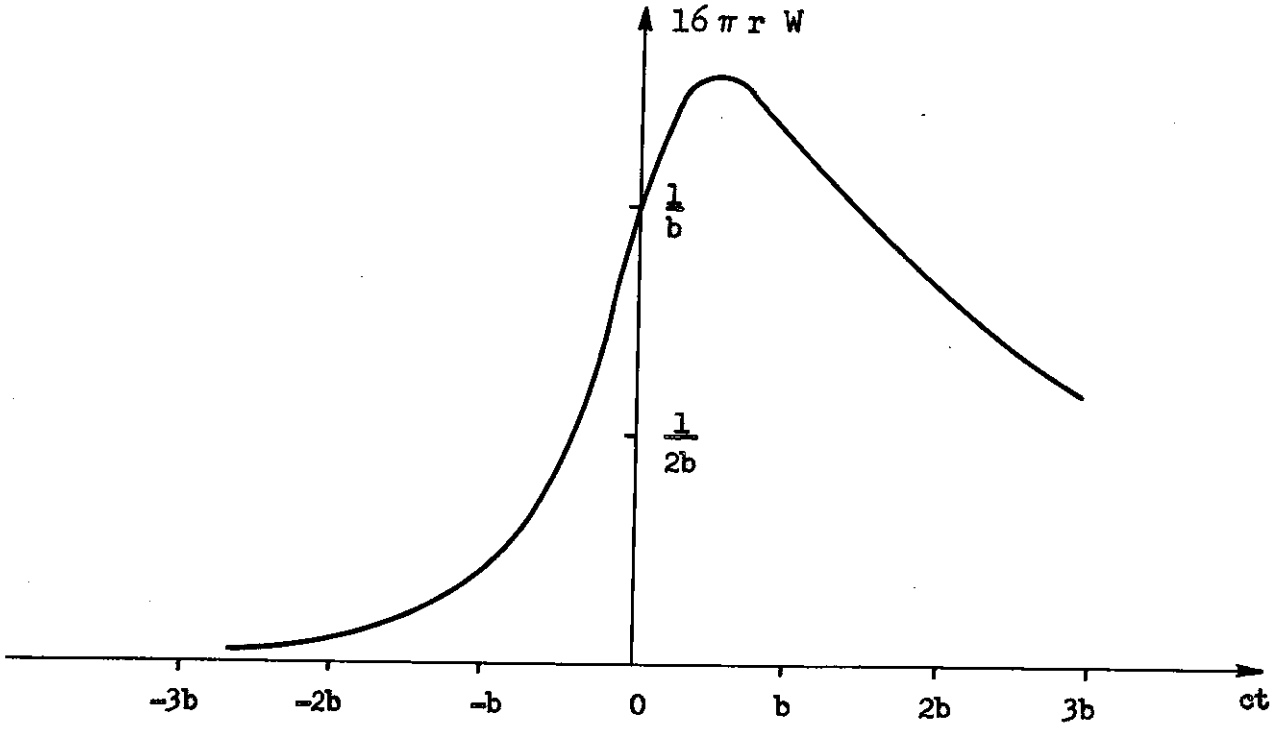

Fig. 11 - Time dependence of the energy density near the edge of the half-plane.

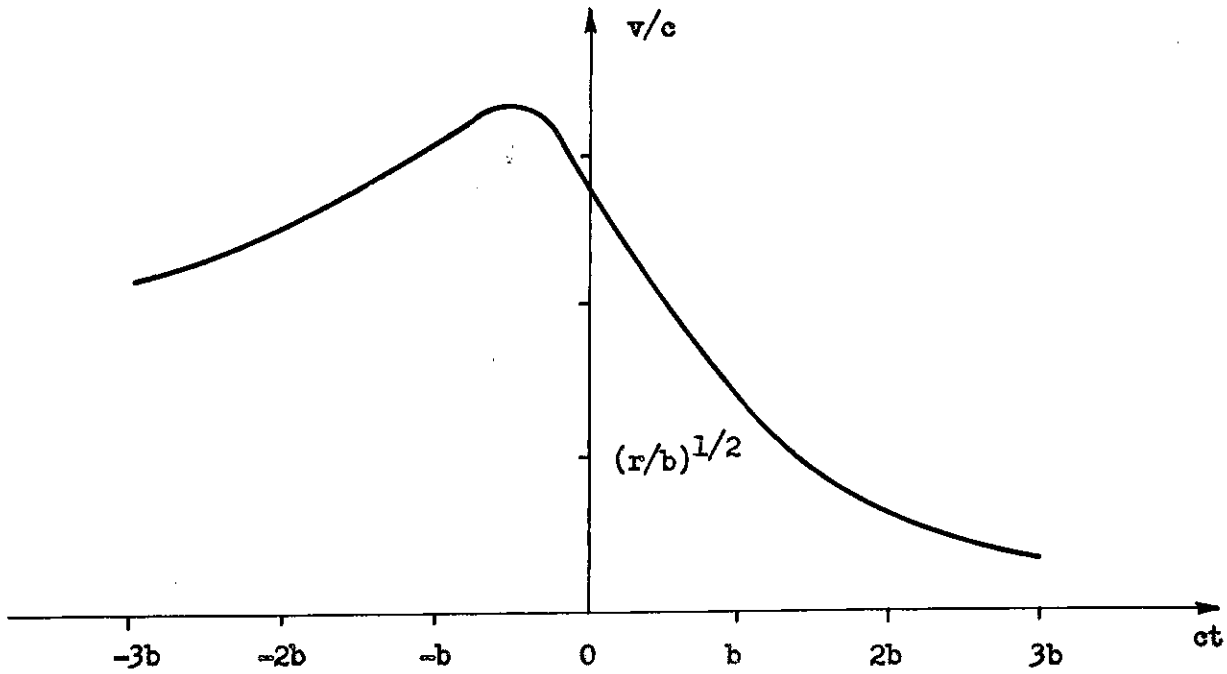

Fig. 12 - Time dependence of the velocity of propagation of the energy near the edge of the half-plane.

The rapid increase of the energy density for $t < 0$, in fig. 11, is clearly due to the arrival of the crest of the incident pulse, whereas its much slower decrease for $t > 0$ shows that part of the incident energy remains near the edge of the half-plane, building up an energy reservoir, before being emitted in the diffracted wave.

This effect also appears in fig. 12: the rapid decrease of v for $t > 0$ gives rise to the slower decrease of the energy contained in the reservoir. The maximum of the energy density is attained for $ct \sim b/2$, there being at this moment a perfect

balance between the energy supply from regions I and II and the energy loss through regions III and IV.

7. Conclusion.

The results obtained in the previous sections allow us to give a complete description of the energy flow as a function of time, in the diffraction process of a pulse of half-width b by a half-plane. The main steps in this process can be described as follows:

For large negative values of the time, there are only slight diffraction effects, due to the head of the pulse . The energy flows smoothly around the half-plane, without formation of any wave fronts.

The main part of the incident pulse reaches the half plane during the interval $-b/c \lesssim t \lesssim b/c$. It gives rise to a strong increase in the energy density near the edge, building up an energy reservoir which, for $t = b/c$, occupies the region $r \lesssim b$, bridging the gap between the transmitted and reflected wave fronts in the neighbourhood of the edge. The velocity of propagation of the energy in the reservoir is small ($v << c$):the energy accumulation has a quasi-electrostatic character. For larger values of the time, as the splitting between the transmitted and reflected wave fronts increases, this energy will be redistributed in the region $r < ct$, giving rise to the dif-

fracted pulse.

The depletion of the energy reservoir does not begin immediately after the arrival of the crest of the incident pulse: there is a time lag of the order of b/c. The appearance of a line where the Poynting vector vanishes first takes place for $t \approx 1.73\ b/c$, showing that only then has the incident energy decreased sufficiently to allow the beginning of backwards emission of the energy contained in the energy reservoir. The line appears at a single point and thereafter it expands with time, separating regions where the energy flows in opposite directions.

The diffracted wave front is formed first near the half plane, where the energy density is greater; it appears later in the opposite half-space. This is due to the wave-guiding properties of the half-plane for transverse magnetic polarization. Another line of zero energy current also appears later in the opposite half-space. It has far less physical significance than the previous one, because the energy density is much weaker in this half-space. As the two lines of zero energy current expand, there remains a separation between them, enabling the energy in the diffracted pulse to flow across the continuation of the half plane. This separation tends to get closed for large values of the time. The same happens to the gap in the diffracted wave front, where it meets the continuation of the half-plane.

Near the junctions between the zero-Poynting-vector lines and the diffracted and geometrical wave fronts, there are

very rapid variations in the energy density and energy current. This effect, insofar as the junctions between the geometrical and diffracted wave fronts are concerned, is the analogue of Fresnel diffraction in monochromatic wave propagation.

For large values of the time, the solution becomes more and more similar to that for a delta-type incident pulse. The diffracted wave tends to become symmetrical with respect to the half-plane, and the whole pattern of the energy flow tends to expand uniformly with velocity c.

* * *

Acknowledgement

The author is greatly indebted to Dr. H. M. Nussenzveig, who suggested and directed the present work, for his guidance, as well as for his assistance during the preparation of this paper. A grant from the National Research Council of Brazil is also gratefully acknowledged.

* * *

REFERENCES

1. To appear in Il Nuovo Cimento.
2. A. Sommerfeld: Z. Math. Phys., 46, 11 (1901).
3. H. Lamb: Proc. Lond. Math. Soc., (2) 8, 422 (1910).
4. F. G. Friedlander: Sound Pulses, (Cambridge University Press, 1958), p. 108.
5. W. Chester: Phil. Trans. Roy. Soc., A 242, 527 (1949).
6. W. Braunbek and G. Laukien: Optik, 9, 174 (1952).
7. B. B. Baker & E. T. Copson: The mathematical theory of Huyghens principle, 2nd ed. (Clarendon Press, 1953). p. 48.
8. C. J. Bouwkamp: Rep. Progr. Phys. 17, 35, 42 (1954).
9. A. Sommerfeld: Mathem. Ann., 47, 317 (1896).
10. H. Bateman: Electrical and Optical Wave-Motion, (Dover Publications, 1955), p. 6.

* * *